Kerr-Microresonator Soliton Frequency Combs at Cryogenic Temperatures

Gregory Moille,[1,2,*] Xiyuan Lu,[1,2] Ashutosh Rao,[1,2] Qing Li,[1,2,3] Daron A. Westly,[1] Leonardo Ranzani,[4] Scott B. Papp,[5,6] Mohammad Soltani,[4] and Kartik Srinivasan[1,7,†]

[1] *Microsystems and Nanotechnology Division, National Institute of Standards and Technology, Gaithersburg, Maryland 20899, USA;*

[2] *Institute for Research in Electronics and Applied Physics and Maryland Nanocenter, University of Maryland, College Park, Maryland 20742, USA*

[3] *Electrical and Computer Engineering, Carnegie Mellon University, Pittsburgh, Pennsylvania 15213, USA;*

[4] *Raytheon BBN Technologies, 10 Moulton Street, Cambridge, Massachusetts 02138, USA*

[5] *Time and Frequency Division, National Institute of Standards and Technology, 385 Broadway, Boulder, Colorado 80305, USA*

[6] *Department of Physics, University of Colorado, Boulder, Colorado 80309, USA;*

[7] *Joint Quantum Institute, NIST–University of Maryland, College Park, Maryland 20742, USA*

(Received 25 June 2019; revised manuscript received 18 August 2019; published 27 September 2019)

We investigate the accessibility and projected low-noise performance of single-soliton Kerr frequency combs in silicon nitride microresonators enabled by operating at cryogenic temperatures as low as 7 K. The resulting 2-orders-of-magnitude reduction in the thermorefractive coefficient relative to room temperature enables direct access to single bright Kerr soliton states through adiabatic frequency tuning of the pump laser while remaining in thermal equilibrium. Our experimental results, supported by theoretical modeling, show that single solitons are easily accessible at temperatures below 60 K for the microresonator device under study. We further demonstrate that the cryogenic temperature primarily impacts the thermorefractive coefficient. Other parameters critical to the generation of solitons, such as quality factor, dispersion, and effective nonlinearity, are unaltered. Finally, we discuss the potential improvement in thermorefractive noise resulting from cryogenic operation. The results of this study open up new directions in advancing chip-scale frequency-comb optical clocks and metrology at cryogenic temperatures.

DOI: 10.1103/PhysRevApplied.12.034057

I. INTRODUCTION

Temporal dissipative Kerr soliton pulses generated in nonlinear microresonators are a promising technology for metrological applications of frequency combs [1]. Their ability to cover a spectral region over an octave [2,3] while operating in a low-noise phase-stable configuration enables new classes of chip-scale photonics components such as optical-frequency synthesizers [4,5], optical clocks [6,7], and microwave generators [8,9]. However, reaching soliton states in practice can be challenging. These states lie on the red-detuned side of the microresonator's pump resonance mode [10,11], for which thermorefractive effects limit stability [12]. This can make accessing soliton states difficult in thermal equilibrium, depending on the properties of the system [2]. Larger-scale resonators, such as MgF_2 crystalline devices [10] and SiO_2 microresonators [13], have sufficiently large thermal conductivity and sufficiently slow thermal time constants to enable soliton generation through slow adjustment of the pump-laser frequency to the appropriate detuning level. In chip-integrated planar microresonators, the thermal time scales are faster and other approaches are typically required. Fast frequency shifting via single-side-band modulators [14], integrated microheaters with fast response times [15], abrupt changes to the pump power level [16], phase modulation of the pump [17], and an auxiliary laser for providing temperature compensation [18] have all been used, while resonators with sufficiently low optical absorption can obviate the need for such methods [19].

Here, we consider a distinct approach, which is to strongly reduce the thermorefractive coefficient $\partial n/\partial T$ of the resonator, making soliton states accessible with slow frequency tuning of the pump laser (Fig. 1). This is accomplished by operating silicon nitride (Si_3N_4) microresonators at cryogenic temperatures ($T \leq 60$ K), where $\partial n/\partial T$ drops significantly [20] (e.g., a 2-orders-of-magnitude reduction at 10 K relative to room temperature). The thermal-expansion coefficient for dielectric thin films also goes down with temperature [21], though for silicon nitride, it starts approximately 10 times lower than $\partial n/\partial T$

*gmoille@umd.edu
†kartik.srinivasan@nist.gov

[22] and is henceforth not considered. After experimentally confirming this large decrease in $\partial n/\partial T$, we examine the resonator dispersion, quality factor, and parametric oscillation threshold, and find that they are largely unaffected by the change in temperature. We then confirm that a reduced thermorefractive coefficient enables straightforward access to single-soliton states and examine how this accessibility changes as the temperature, and thus $\partial n/\partial T$, is increased. Our experimental results are in good correspondence with the theory developed in Ref. [2], where the Lugiato-Lefever equation (LLE) for modeling Kerr dynamics is combined with a simple thermal model. Outside of this demonstration of soliton cryocombs, we theoretically consider the implications of cryogenic operation on soliton stability. In particular, we consider how reduced thermorefractive effects can lower carrier-envelope offset frequency noise [23] by several orders of magnitude.

II. RESULTS AND DISCUSSION

A. Thermal accessibility of soliton states: Model

To understand the thermal accessibility of Kerr soliton states in a microresonator, schematically described in Fig. 1(a), we employ the theoretical model presented in Ref. [2] as a base for our study. Due to the large difference in time scales for Kerr and thermal dynamics, thermorefractive effects can be added to the LLE model in a two-step fashion. First, the LLE is simulated to determine the behavior of the comb power as a function of the pump-laser detuning with respect to its adjacent cavity mode, such that a positive detuning corresponds to a red-detuned pump laser [see Fig. 1(b)]. As the pump frequency is swept across the transition from chaotic modulation-instability (MI) states to the soliton regime, the large drop in comb power results in a sudden temperature change, with a resulting shift of the cavity resonance due to the thermorefractive effect. A simple thermal model results in a linear solution with a slope $K_{\text{eff}} \propto (\partial n/\partial T)^{-1}$. When the solution of the thermal model intersects a soliton step, the shift of the cavity mode due to the temperature change upon entering the soliton regime is small enough that the system remains in a soliton state. Since $\partial n/\partial T$ is temperature dependent, soliton steps that are inaccessible at room temperature can be accessed at cryogenic temperatures, as shown in Fig. 1(b), for which $\partial n/\partial T$ is sufficiently small.

B. Thermorefractive coefficient, cavity *Q*, and comb threshold versus temperature

The device that we investigate is a microring resonator [inset of Fig. 2(a)] made of 617-nm-thick Si_3N_4 with a 3 μm SiO_2 bottom layer above a Si substrate, without any top cladding layer. The other geometrical dimensions of the microring are an outer ring radius $R = 23$ μm and a ring width RW = 1850 nm, resulting in a dispersion profile that supports octave-spanning soliton comb states, as accessed through fast frequency sweeping in Ref. [14]. Such rapid pump-frequency adjustment is a necessity due to the room-temperature thermal dynamics

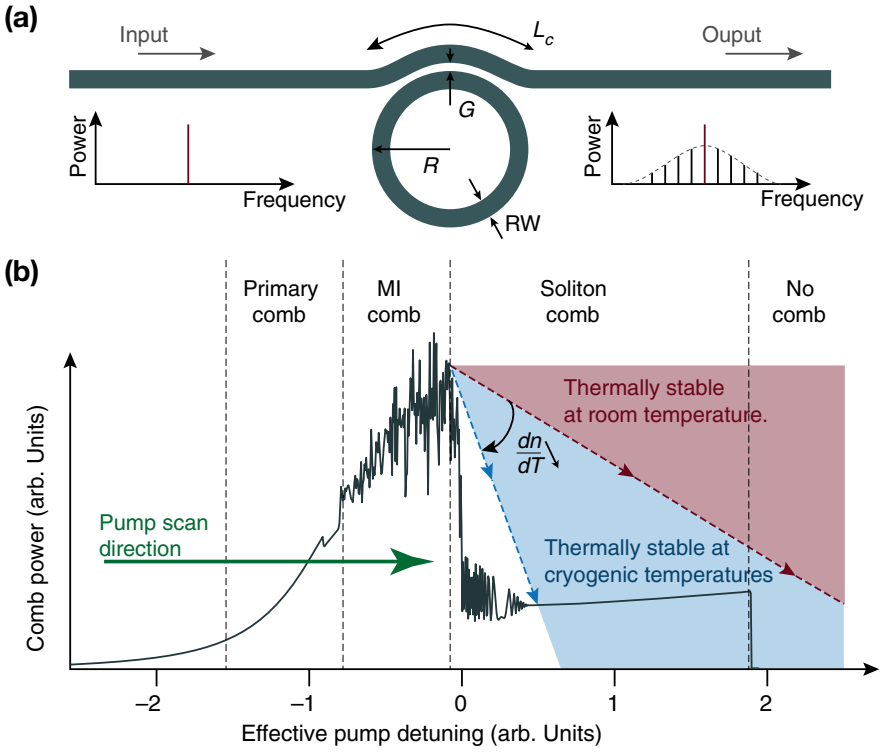

FIG. 1. (a) A schematic of the microring studied, where a single-frequency continuous-wave laser at the input results in a soliton microcomb at the output due to the $\chi^{(3)}$ nonlinearity of the resonator: RW, ring width; G = gap; R, radius; L_c, coupling length. (b) The thermal accessibility of soliton states. The black line shows the LLE-simulated comb power (i.e., the integrated power in the comb with the pump line filtered out) as a function of the laser-pump-mode detuning, while the red and blue dashed lines represent a range of solutions to the thermorefractive model as the temperature (and hence $\partial n/\partial T$) is decreased. The intersection of the thermal model solution and the soliton step of the LLE simulation determines whether that soliton state is thermally stable. MI, modulation instability.

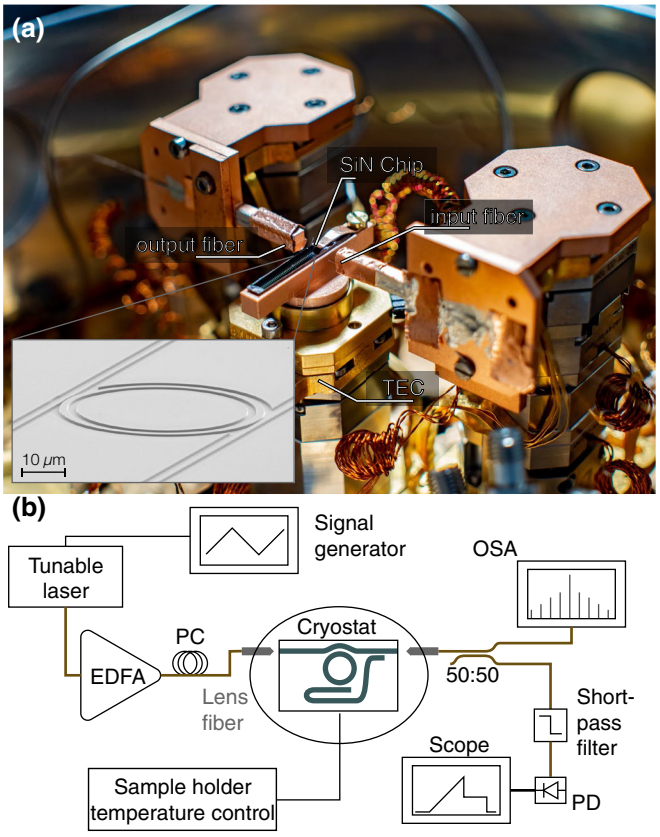

FIG. 2. (a) A photograph of the cryostat interior with input and output fiber coupling to the Si_3N_4 chip. The coupling to the ring is made with two waveguides to extract different portions of the comb spectrum and they are combined before the output port through an on-chip dichroic element. The chip sits on a copper mount affixed to a feedback-controlled heater stage that enables the temperature to be varied from 6 K to 90 K without adjusting the cooling power to the cryostat. The inset is a scanning-electron-microscopy image of an individual microring resonator. (b) The experimental setup for soliton generation at cryogenic temperature: OSA, optical spectrum analyzer; PD, photodiode; PC, polarization controller; EDFA, erbium-doped fiber amplifier.

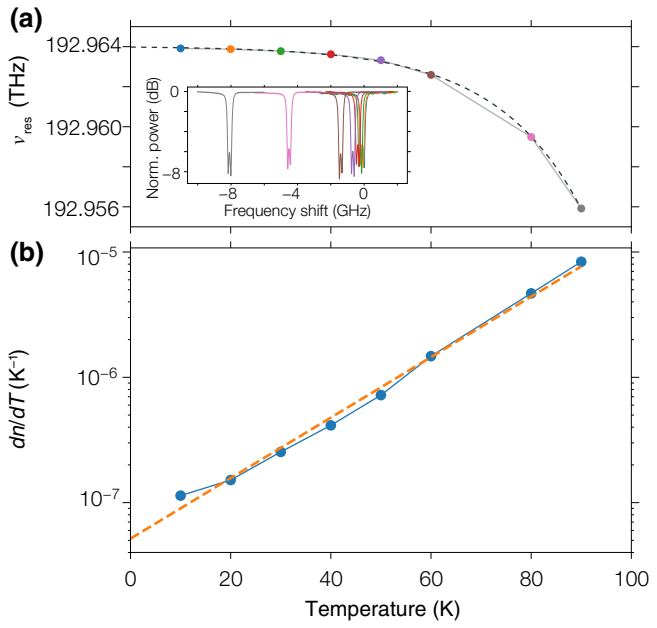

FIG. 3. (a) The spectral shift of the microring resonator pump mode with temperature. The dashed line corresponds to the exponential fit used to retrieve $\partial n/\partial T$. The inset represents the measured resonance profile, a doublet that is fitted using the model from Ref. [24]. (b) Variation of the thermorefractive coefficient of the system with temperature. The dashed line corresponds to the exponential trend. The uncertainties are within the size of the markers.

preventing single-soliton accessibility through adiabatic tuning of the frequency. We place the chip inside a 20-cm-diameter chamber within a closed-cycle cryostat with a base temperature $T \leqslant 5$ K (Fig. 2). The sample is mounted on a copper sample holder that is affixed to a temperature-controlled stage that incorporates a resistive heater with an embedded temperature sensor and closed-cycle control. Hence, the temperature of the sample can be tuned between 6 K and 100 K without adjusting the cooling power to the cryostat. The sample is optically addressed using lensed optical fibers and special care is taken to thermally sink both the fibers and the sample, to limit adverse heating effects when significant optical powers are coupled into the system.

We first experimentally examine the thermorefractive coefficient, which is retrieved by measuring the frequency shift of a resonance $\partial\nu/\partial T$ with temperature from 10 K up to 90 K [Fig. 3(a)]; in particular, probing the mode used later as the pumped one to create a microcomb. From the mode frequency shift and its relation with the thermorefractive coefficient $\partial n/\partial T \equiv (\partial\nu_0/\partial\tilde{n})^{-1}\,\partial\nu_0/\partial T$, with $\partial\nu/\partial n = -92.57$ THz (calculated using a finite-element method (FEM) eigensolver), $\partial n/\partial T$ of the system is determined. The benefit of going to cryogenic temperature is clear as the thermorefractive coefficient of the system drops by 2 orders of magnitude in going from 90 K to 10 K [Fig. 3(b)] and exhibits more than a factor of 2 difference between 90 K and its value reported at room temperature, $\partial n/\partial T|_{300\ \mathrm{K}} = 2.45 \times 10^{-5}\ \mathrm{K}^{-1}$ [25]. These results are consistent with data reported on the cryogenic behavior of the thermorefractive coefficient for both Si_3N_4 and SiO_2 [20].

To check that the primary influence of a cryogenic temperature on soliton accessibility is through the reduced $\partial n/\partial T$, it is essential to verify that no other parameters critical to soliton formation and stability significantly vary with temperature. First, we consider whether the temperature influences the resonator dispersion, through measurement of its mode frequencies from approximately 180 THz

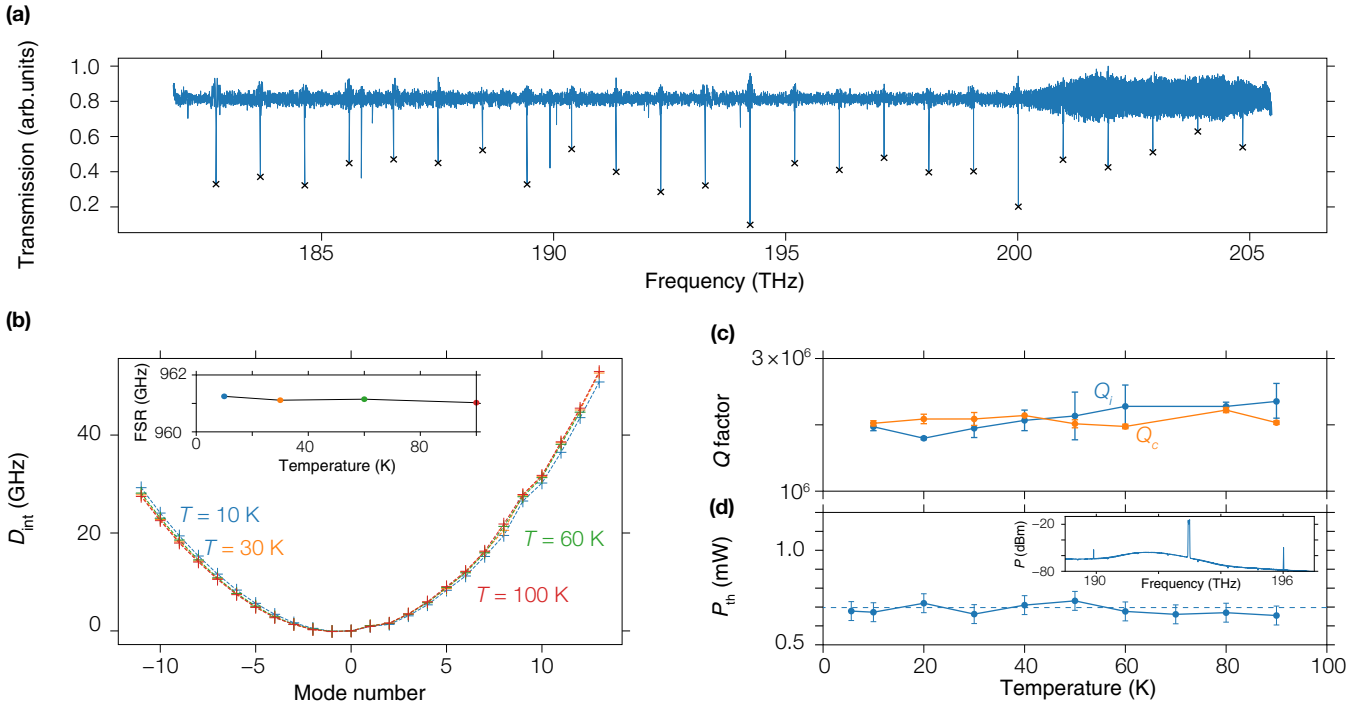

FIG. 4. (a) The linear transmission of the ring resonator at 60 K. The crosses mark the first-order mode family of interest for broad soliton comb generation. (b) The integrated dispersion obtained from the linear transmission data such as that in (a) as a function of the mode number and at different temperatures. For the frequency range considered, the dispersion is nearly quadratic. The inset corresponds to the change in the extracted FSR with temperature. The uncertainties are within the size of the markers. (c) The behavior of the intrinsic (blue) and coupling (orange) quality factor with temperature. The error bars represent 95% confidence intervals from a nonlinear least-squares fit to the data. (d) The threshold power P_{th} for optical parametric oscillation (OPO) as a function of temperature, where the error bars are one-standard-deviation values due to variation in the fiber insertion loss. The inset corresponds to the optical spectrum of the first OPO side bands obtained at P_{th}.

to approximately 205 THz [Fig. 4(a)]. These measurements allow us to retrieve the free spectral range (FSR) for the targeted mode family, as well as the integrated dispersion, given by $D_{int} = \nu_\mu - (\nu_0 + D_1 \times \mu)$, where μ represents the mode number relative to the pumped-mode frequency ν_0 and ν_μ is the frequency of the μ^{th} mode and D_1 is the resonator FSR. For both, no significant change is observed with temperature [Fig. 4(b)], which indicates that the thermorefractive coefficient is quasi-non-dispersive in the frequency band of interest. Given the sensitivity of dispersion on the resonator geometry, this suggests that the ring dimensions are also largely unchanged with temperature and supports our assumption that thermal-expansion effects can be neglected over the temperature range studied. This claim is further supported by measurement of the intrinsic and coupled quality factors, which are found to be unaltered from 10 K to 90 K [Fig. 4(c)], suggesting that the geometry is not changing significantly as the resonator-waveguide coupling is sensitive to relatively small geometric changes. Finally, by increasing the pump-laser power while keeping a fixed detuning on the blue side of the pump-cavity resonance, we observe optical-parametric oscillation (OPO), as seen in the inset to Fig. 4(d). We find that the threshold power for OPO is approximately constant with temperature. As the quality factor and the power threshold are unchanged with temperature, we can conclude that the nonlinear coefficient n_2 of the Si_3N_4 remains unchanged; hence only the thermorefractive coefficient is impacted by the cryogenic temperatures.

C. Soliton generation and step length versus temperature

We measure the soliton dynamics of the system by pumping the resonance at $\nu_0 \approx 192.96$ THz that is used to characterize the quality factor, the power threshold, and the thermal shift. Applying an in-waveguide power of $P_{pmp} \approx$ 100 mW, a single-soliton state is easily reached through adiabatic tuning of the pump-laser frequency due to the drop of the thermorefractive coefficient and the spectrum of the resulting microcomb is reported in Fig. 5(a), exhibiting the characteristic and expected $sech^2$ envelope. The measured microcomb spectrum is in good agreement with the spectral envelope predicted by simulations of the LLE performed using an open-source software package

[26]. One exception is the lack of a low-frequency dispersive wave around 135 THz, which is not present experimentally. We believe that this is most likely a technical issue that is a result of our measurement. Due to the small space available in between the cryostat radiation shield and the fiber feedthrough that connects the vacuum space to the outside laboratory, the SMF28e fibers [27] running to and from the comb chip undergo tight bends. As has been seen in other literature [28], bend diameters below 40 mm can cut off long-wavelength light above 2 μm (below 150 THz).

We examine a range of cryogenic temperatures for which a single soliton is accessible and find the soliton step width for the corresponding temperature. For this experiment, we measure the comb power, i.e., the output power when the pump is filtered out, as a function of the temperature and for an in-waveguide pump power of $P_{\mathrm{pmp}} \approx 40$ mW [Fig. 5(b)]. This power level is chosen based upon simulations that indicate a favorable operating point for single-soliton generation. The comb-power traces [Fig. 5(b)] indicate a transition from states accessible on the blue-detuned side of the resonance (comb power increasing) to the abrupt soliton steps on the red-detuned side (we note that the detector bandwidth of 500 kHz precludes observation of the fast intensity variations expected for chaotic states on the blue-detuned side, as seen in the LLE simulation). It is clear from these traces that the single-soliton step is observable up to 60 K and the step width is wider for lower temperatures, making the soliton regime more accessible. It is clear from the comb-power traces in Figs. 5(b) that the single-soliton step is observable up to 60 K and that the step width is wider for lower temperatures, making the soliton regime more accessible. At a temperature of 60 K, a soliton step at higher comb power is observed, corresponding to a higher number of soliton pulses in the cavity. We emphasize the time scale of the pump-frequency sweep (milliseconds), which is orders of magnitude slower than the thermal lifetime in our system, usually on the order of tenths of a microsecond [16]. In Ref. [2], it was shown that under such slow frequency sweeps, only multisoliton states were accessible at room temperature unless a very specific condition of temperature compensation via coupling to an adjacent optical mode was possible. Here, we consider soliton accessibility at cryogenic temperatures.

To further investigate the single-soliton dynamics at cryogenic temperatures, we compare the measured single-soliton step length with the temperature and the theoretical

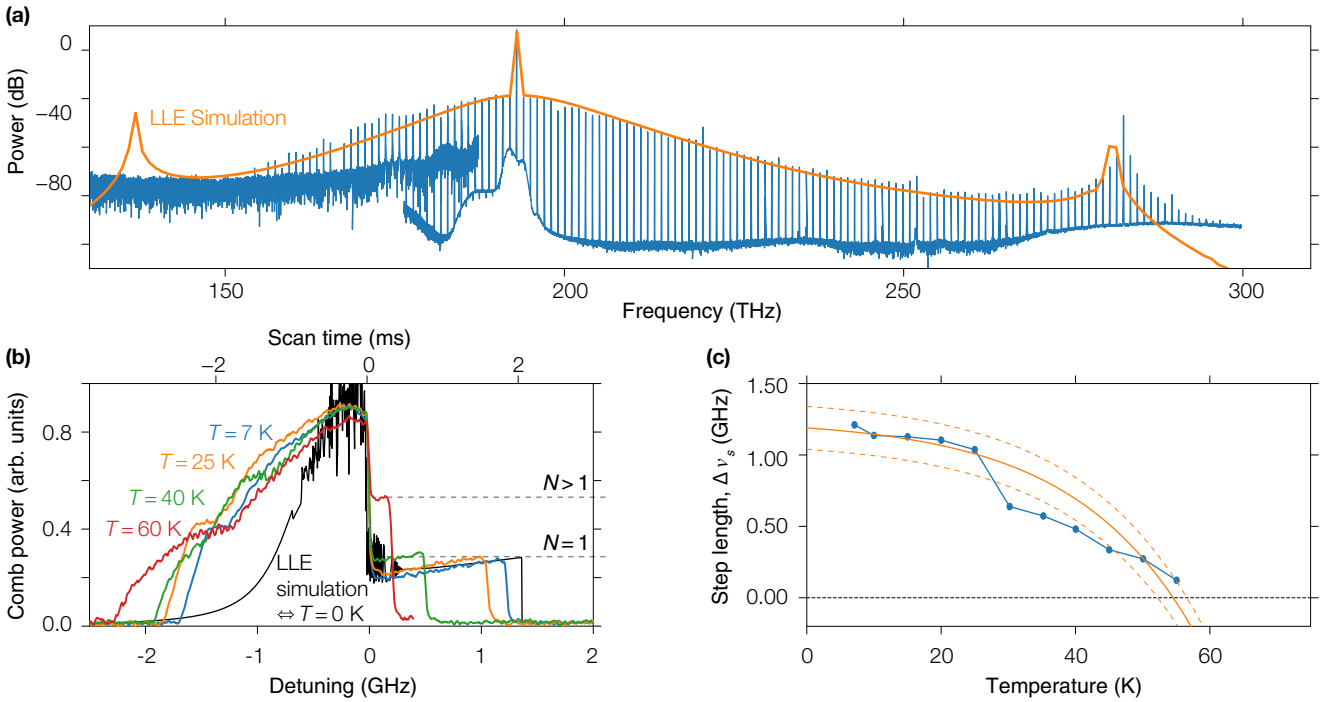

FIG. 5. (a) The measured (blue) and simulated (orange) single-soliton frequency combs obtained at $T \approx 7$ K with a pump power of 100 mW in the waveguide. The spectrum is acquired using two optical-spectrum analyzers. The noise floor of the instrument for acquiring the lower-frequency section is about 20 dB higher than that which acquires the higher-frequency section. (b) The comb power versus the detuning $\nu_0 - \nu_{\mathrm{pmp}}$ obtained at different temperatures. The black line corresponds to the LLE simulation. (c) The measured soliton step length (blue) versus temperature, compared to theoretical values assuming nominal parameters from the experiment (solid orange line). In addition, we plot a range of theoretical values (dashed orange lines) defined by ± 1 dB variation in the pump power, which represents the observed fluctuation in insertion loss during the experiment.

one obtained through the thermal-stability study presented in ref [2]. Based on that work, one can write the soliton step length as follows:

$$\Delta\nu_s(T) = \Delta\nu_s^0 - (1-\eta)K_{\text{eff}}^{-1}(T), \tag{1}$$

where $\Delta\nu_s(T)$ is the soliton step length at temperature T, $\Delta\nu_s^0$ is the theoretically predicted step length from the LLE (in the absence of thermal effects, i.e., at $T=0$), η is the ratio between the peak of the MI comb power and the soliton step power, and K_{eff} describes the thermal frequency shift such that $K_{\text{eff}}^{-1} = 2\frac{\omega_0 t_R}{n_g K_c}\frac{\kappa_a}{\kappa} \times \frac{\partial n}{\partial T}$, where κ_a/κ is the ratio of the linear absorption rate to the total loss rate. Other parameters include a group index $n_g = 2.0669$, a round-trip time $t_R = 0.996$ ps obtained from FEM simulation, $\Delta\nu_s^0 = 1.23$ GHz obtained from LLE simulation, and thermal conductance $K_c = 2.86 \times 10^{-4}$ W/K. To match our experimental data, the prefactor in front of $\partial n/\partial T$ in K_{eff}^{-1} needs to be about a factor of 2 larger than that calculated in Ref. [2]. This difference is perhaps not surprising, because of the different thermal environment (the microring is now in vacuum instead of air), the potential change in the thermal conductivity of Si_3N_4 and SiO_2 at cryogenic temperatures, and the varying fraction of loss due to absorption from device to device. From the thermal-plus-LLE model, we retrieve the theoretical behavior of the soliton step length [Fig. 5(c)], which is consistent with the experimental results [particularly when accounting for potential variation in the pump power due to changes in coupling; see the dashed lines in Fig. 5(c)]. This also shows that above 60 K, the single-soliton state is not thermally stable anymore ($\Delta\nu_s < 0$), which is also consistent with experimental observation.

D. Potential impact of reduced thermorefractive noise on soliton-microcomb stability

Finally, an essential consequence of the drop in the thermorefractive coefficient at cryogenic temperatures is the potential to reduce thermorefractive noise. Indeed, the resonance frequencies of the different modes of the microring depend on the material refractive index. Hence, thermal fluctuation leads to frequency noise through the thermorefractive coefficient. The mean thermal fluctuation can be derived from thermodynamics as $\langle\delta T^2\rangle = k_B T^2/CV_m\rho$, where C is the heat capacity, V_m is the optical-mode volume of the mode m, k_B is Boltzmann's constant, and ρ is the density of the resonator material. The thermal fluctuations are directly linked to the variation of the resonance frequency $\delta\nu/\nu = -n^{-1}(\partial n/\partial T)\delta T$, which can be reformulated as the spectral density of optical fluctuations:

$$S_\nu = \left(\nu_0 n^{-1}\frac{\partial n}{\partial T}\right)^2 S_T, \tag{2}$$

where S_T the spectral density of thermal fluctuations. This last physical quantity has been the subject of investigation in different works and several analytical models have been reported. The two models that will be used in this work, and that have been demonstrated to match Si_3N_4 experimental data well for different Fourier-frequency spectral windows [29], are the approximation of a homogeneous cavity within a heat bath [30] and the approximation of the thermal decomposition method [31]. The former can be written as follows:

$$S_T(\omega) = \frac{k_B T^2}{\sqrt{\pi^3\kappa\rho C\omega}}\sqrt{\frac{1}{2m}} \times \frac{1}{R\sqrt{d_r^2 - d_z^2}}\frac{1}{\left(1+(\omega\tau_d)^{3/4}\right)^2}, \tag{3}$$

where $R = 23$ μm is the ring radius, d_z and d_r are the half-widths of the fundamental mode with the azimuthal mode order $m = 159$ in the r and z directions, respectively, $\tau_d = (\pi^{3/4}/4^{1/3})(\rho C/\kappa)d_z^2$, ω is the Fourier frequency, and κ is the thermal conductivity of the material. We use thermal properties that one can find in the literature, including the specific heat capacity $C = 800\ \text{J kg}^{-1}\text{K}^{-1}$, $\kappa = 30\ \text{W m}^{-1}\text{K}^{-1}$, and the density $\rho = 3.29 \times 10^3\ \text{kg m}^{-3}$.

The second model used here can be written as follows:

$$S_T(\omega) = \frac{k_B T^2 R^2}{12\kappa V_m} \times \left(1 + \left(\frac{R^2\rho C\omega}{3^{5/2}\kappa}\right)^{3/2} + \frac{1}{6}\left(\frac{R^2\rho C\omega}{8m^{1/3}\kappa}\right)^2\right)^{-1}, \tag{4}$$

where $V_m = 1 \times 10^{-16}\ \text{m}^{-3}$ is the effective volume.

From Eqs. (2)–(4), the improvement at cryogenic temperatures is obvious, as the spectral density of frequency fluctuation scales with $(\partial n/\partial T)^2\, T^2$, and Fig. 6(a) shows an improvement of 4 orders of magnitude in the normalized spectral density of optical fluctuation $\sqrt{S_\nu}/\nu_0$ compared to its value at room temperature. However, even if the spectral density of noise is largely reduced by working at cryogenic temperatures, the Q of Si_3N_4 rings such as those we study is generally too low to consider them as viable candidates for reference cavities [32]. Going forward, recent improvements in the Q of thick Si_3N_4 [33–35] resonators, as well as earlier work on thin Si_3N_4 resonators with quality factors approaching 10^8 [36], suggest the future potential to combine such higher Q with cryogenic operation toward reference-cavity applications.

Applications of octave-spanning soliton frequency combs typically require a stabilized carrier-envelope offset frequency (f_{CEO}), which is often determined through the f-$2f$ beat-note detection scheme. However, fluctuations in this beat note can arise from thermal noise, setting a limit

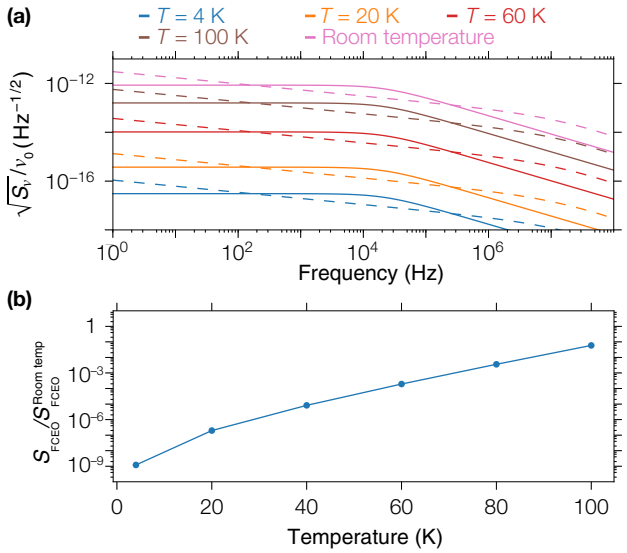

FIG. 6. The calculation of (a) the fractional spectral density of optical-frequency fluctuations $\sqrt{S_\nu}/\nu_0$ and (b) the ratio of the spectral density of the soliton-comb carrier-envelope offset frequency fluctuations S_{FCEO} at a given temperature to the value at room temperature. We assume the experimental values of $\partial\nu_0/\partial T$ from Fig. 3 and other parameters from Ref. [23].

on the metrological applications of such combs [23]. From Ref. [23], one can link the spectral density of thermal noise to that of f_{CEO}, such that

$$S_{\mathrm{FCEO}}(\omega) = p^2\eta_{\mathrm{rep}}^2 S_T(\omega), \tag{5}$$

where $p = 192$ is the pumped-comb mode number and η_{rep} is given by the following:

$$\eta_{\mathrm{rep}} = \left(\frac{\partial f_{\mathrm{rep}}}{\partial\nu_0} - \frac{\partial f_{\mathrm{rep}}}{\partial\Delta}\right)\frac{\partial\nu_0}{\partial T}. \tag{6}$$

Like the spectral density of optical-frequency fluctuations, the spectral density of f_{CEO} fluctuations scales with $\left(\frac{\partial n}{\partial T}\right)^2 T^2$ and thus should strongly benefit from cryogenic temperature operation, both from the reduction in temperature and the drop of the thermorefractive coefficient. This leads to a predicted improvement in the density of noise fluctuations of close to 9 orders of magnitude [Fig. 6(b)].

III. CONCLUSION

In conclusion, we demonstrate soliton generation at cryogenic temperatures in Si_3N_4 microrings. This is enabled by the drop in the thermorefractive coefficient, which we measure to be more than 2 orders of magnitude smaller compared to the room-temperature value, quenching the thermal bistability and leading to thermally stable soliton states. In addition, measurement of critical parameters such as quality factors, dispersion, and the threshold power is performed at different temperatures and leads to the conclusion that the cryogenic temperature primarily modifies the thermorefractive coefficient. Moreover, the ability to strongly suppress thermorefractive effects may enable experimental verifications of a number of theoretical predictions that are based on studies of the Kerr dynamics alone. We further validate the theory introduced in Ref. [2] by varying the temperature of the device, which alters the thermorefractive coefficient and results in a change of the soliton step length that is consistent with the theory. Finally, we theoretically investigate the expected reduction in noise, both for the spectral density of optical-frequency fluctuations, which is important for reference-cavity applications, and the spectral density of carrier-envelope offset frequency fluctuations, which has a significant impact on the stability of phase-locked octave-spanning microcombs. For both figures of merit, we expect an improvement of several orders of magnitude, due to both the drop in temperature and the drop in the thermorefractive coefficient. This suggests that other noise sources may be the ultimate limiting noise factor when Si_3N_4 microrings are operated at cryogenic temperature. Although cryogenics adds a level of complexity beyond experiments done in ambient, the potential for such temperatures to be naturally reached in some satellite applications, as well as recent advances in miniaturized cryocoolers [37], indicates significant potential impact in the implementation of low-noise and stable compact clocks and metrology systems.

ACKNOWLEDGMENTS

This work is supported by the Defense Advanced Research Projects Agency (DARPA) Direct On-Chip Digital Optical Synthesizer (DODOS), Atomic Clock with Enhanced Stability (ACES), and NIST-on-a-Chip programs. G.M., X.L., and Q.L. acknowledge support under the Cooperative Research Agreement between the University of Maryland and the NIST–Physical Measurement Laboratory (PML), through Award No. 70NANB10H193. The authors thank Tara Drake from NIST Boulder and Amit Agrawal from NIST Gaithersburg for helpful discussions.

[1] Tobias J. Kippenberg, Alexander L. Gaeta, Michal Lipson, and Michael L. Gorodetsky, Dissipative Kerr solitons in optical microresonators, Science **361**, eaan8083 (2018).

[2] Qing Li, Travis C. Briles, Daron A. Westly, Tara E. Drake, Jordan R. Stone, B. Robert Ilic, Scott A. Diddams, Scott B. Papp, and Kartik Srinivasan, Stably accessing octave-spanning microresonator frequency combs in the soliton regime, Optica **4**, 193 (2017).

[3] Martin H. P. Pfeiffer, Clemens Herkommer, Junqiu Liu, Hairun Guo, Maxim Karpov, Erwan Lucas, Michael Zervas, and Tobias J. Kippenberg, Octave-spanning dissipative Kerr soliton frequency combs in Si_3N_4 microresonators, Optica **4**, 684 (2017).

[4] R. Holzwarth, Th. Udem, T. W. Hänsch, J. C. Knight, W. J. Wadsworth, and P. St. J. Russell, Optical Frequency Synthesizer for Precision Spectroscopy, Phys. Rev. Lett. **85**, 2264 (2000).

[5] Daryl T. Spencer *et al.*, An optical-frequency synthesizer using integrated photonics, Nature **557**, 81 (2018).

[6] Andrew D. Ludlow, Martin M. Boyd, Jun Ye, E. Peik, and P. O. Schmidt, Optical atomic clocks, Rev. Mod. Phys. **87**, 637 (2015).

[7] Tara E. Drake, Travis C. Briles, Jordan R. Stone, Daryl T. Spencer, David R. Carlson, Daniel D. Hickstein, Qing Li, Daron Westly, Kartik Srinivasan, Scott A. Diddams, and Scott B. Papp, Terahertz-Rate Kerr-Microresonator Optical Clockwork, Phys. Rev. X **9**, 031023 (2019).

[8] T. M. Fortier, M. S. Kirchner, F. Quinlan, J. Taylor, J. C. Bergquist, T. Rosenband, N. Lemke, A. Ludlow, Y. Jiang, C. W. Oates, and S. A. Diddams, Generation of ultrastable microwaves via optical frequency division, Nat. Photonics **5**, 425 (2011).

[9] Erwan Lucas, Pierre Brochard, Romain Bouchand, Stéphane Schilt, Thomas Süudmeyer, and Tobias J. Kippenberg, Ultralow-Noise Photonic Microwave Synthesis Using a Soliton Microcomb-Based Transfer Oscillator, arXiv:1903.01213 (2019).

[10] T. Herr, V. Brasch, J. D. Jost, C. Y. Wang, N. M. Kondratiev, M. L. Gorodetsky, and T. J. Kippenberg, Temporal solitons in optical microresonators, Nat. Photonics **8**, 145 (2013).

[11] Cyril Godey, Irina V. Balakireva, Aurélien Coillet, and Yanne K. Chembo, Stability analysis of the spatiotemporal Lugiato-Lefever model for Kerr optical frequency combs in the anomalous and normal dispersion regimes, Phys. Rev. A. **89**, 063814 (2014).

[12] Tal Carmon, Lan Yang, and Kerry J. Vahala, Dynamical thermal behavior and thermal self-stability of microcavities, Opt. Express **12**, 4742 (2004).

[13] Xu Yi, Qi-Fan Yang, Ki Youl Yang, Myoung-Gyun Suh, and Kerry Vahala, Soliton frequency comb at microwave rates in a high-Q silica microresonator, Optica **2**, 1078 (2015).

[14] Travis C. Briles, Jordan R. Stone, Tara E. Drake, Daryl T. Spencer, Connor Fredrick, Qing Li, Daron Westly, B. R. Ilic, Kartik Srinivasan, Scott A. Diddams, and Scott B. Papp, Interlocking Kerr-microresonator frequency combs for microwave to optical synthesis, Opt. Lett. **43**, 2933 (2018).

[15] Chaitanya Joshi, Jae K. Jang, Kevin Luke, Xingchen Ji, Steven A. Miller, Alexander Klenner, Yoshitomo Okawachi, Michal Lipson, and Alexander L. Gaeta, Thermally controlled comb generation and soliton modelocking in microresonators, Opt. Lett. **41**, 2565 (2016).

[16] Victor Brasch, Michael Geiselmann, Martin H. P. Pfeiffer, and Tobias J. Kippenberg, Bringing short-lived dissipative Kerr soliton states in microresonators into a steady state, Opt. Express **24**, 29312 (2016).

[17] Daniel C. Cole, Jordan R. Stone, Miro Erkintalo, Ki Youl Yang, Xu Yi, and Kerry J. Vahala, and Scott B. Papp, Kerr-microresonator solitons from a chirped background, Optica **5**, 1304 (2018).

[18] Shuangyou Zhang, Jonathan M. Silver, Leonardo Del Bino, Francois Copie, Michael T. M. Woodley, George N. Ghalanos, Andreas Ø. Svela, Niall Moroney, and Pascal Del'Haye, Sub-milliwatt-level microresonator solitons with extended access range using an auxiliary laser, Optica **6**, 206 (2019).

[19] Junqiu Liu, Erwan Lucas, Jijun He, Arslan S. Raja, Rui Ning Wang, Maxim Karpov, Hairun Guo, Romain Bouchand, and Tobias J. Kippenberg, Photonic microwave oscillators based on integrated soliton microcombs, arXiv:1901.10372 (2019).

[20] Ali W. Elshaari, Iman Esmaeil Zadeh, Klaus D. Jons, and Val Zwiller, Thermo-optic characterization of silicon nitride resonators for cryogenic photonic circuits, IEEE Photonics J. **8**, 1 (2016).

[21] Jack W. Ekin, *Experimental Techniques for Low-Temperature Measurements* (Oxford University Press, Oxford, 2006).

[22] A. Kaushik, H. Kahn, and A. H. Heuer, Wafer-level mechanical characterization of silicon nitride MEMS, J. Microelectromech. Syst. **14**, 359 (2005).

[23] Tara E. Drake, Jordan R. Stone, Travis C. Briles, and Scott B. Papp, Thermal decoherence and laser cooling of Kerr microresonator solitons, arXiv:1903.00431 (2019).

[24] M. Borselli, T. J. Johnson, and O. Painter, Beyond the Rayleigh scattering limit in high-Q silicon microdisks: Theory and experiment, Opt. Express **13**, 1515 (2005).

[25] Amir Arbabi and Lynford L. Goddard, Measurements of the refractive indices and thermo-optic coefficients of $rmSi_3N_4$ and SiO(x) using microring resonances, Opt. Lett. **38**, 3878 (2013).

[26] Gregory Moille, Qing Li, and Xiyuan Lu, and Kartik Srinivasan, PYLLE: A fast and user friendly Lugiato-Lefever equation solver, J. Res. Natl. Institute Standards Technol. **124**, 124012 (2019).

[27] Certain commercial items are identified in this paper to foster understanding. Such identification does not imply recommendation or endorsement by NIST; nor does it imply that the items identified are necessarily the best available for the purpose.

[28] Paulina S. Kuo, Using silica fiber coupling to extend superconducting nanowire single-photon detectors into the infrared, OSA Continuum **1**, 1260 (2018).

[29] Guanhao Huang, Erwan Lucas, Junqiu Liu, Arslan S. Raja, Grigory Lihachev, Michael L. Gorodetsky, Nils J. Engelsen, and Tobias J. Kippenberg, Thermorefractive noise in silicon-nitride microresonators, Phys. Rev. A **99**, 061801 (2019).

[30] N. M. Kondratiev and M. Gorodetsky, Thermorefractive noise in whispering gallery mode microresonators: Analytical results and numerical simulation, Phys. Lett. A **382**, 2265 (2018).

[31] Andrey B. Matsko, Anatoliy A. Savchenkov, and Nan Yu, Lute Maleki, Whispering-gallery-mode resonators as frequency references I fundamental limitations, J. Opt. Soc. Am. B. **24**, 1324 (2007).

[32] Julius de Hond, Nataly Cisternas, Graham Lochead, and N. J. van Druten, Medium-finesse optical cavity for the stabilization of Rydberg lasers, Appl. Opt. **56**, 5436 (2017).

[33] Yi Xuan, Yang Liu, Leo T. Varghese, Andrew J. Metcalf, Xiaoxiao Xue, Pei-Hsun Wang, Kyunghun Han, Jose A. Jaramillo-Villegas, Abdullah Al Noman, Cong Wang, Sangsik Kim, Min Teng, Yun Jo Lee, Ben Niu, Li Fan, Jian Wang, Daniel E. Leaird, Andrew M. Weiner, and Minghao Qi, High-Q silicon nitride microresonators exhibiting low-power frequency comb initiation, Optica **3**, 1171 (2016).

[34] Xingchen Ji, Felippe A. S. Barbosa, Samantha P. Roberts, Avik Dutt, Jaime Cardenas, Yoshitomo Okawachi, Alex Bryant, Alexander L. Gaeta, and Michal Lipson, Ultra-low-loss on-chip resonators with sub-milliwatt parametric oscillation threshold, Optica **4**, 619 (2017).

[35] Junqiu Liu, Arslan S. Raja, Maxim Karpov, Bahareh Ghadiani, Martin H. P. Pfeiffer, Botao Du, Nils J. Engelsen, Hairun Guo, Michael Zervas, and Tobias J. Kippenberg, Ultralow-power chip-based soliton microcombs for photonic integration, Optica **5**, 1347 (2018).

[36] Daryl T. Spencer, Jared F. Bauters, Martijn J. R. Heck, and John E. Bowers, Integrated waveguide coupled Si_3N_4 resonators in the ultrahigh-Q regime, Optica **1**, 153 (2014).

[37] T. Conrad, B. Schaefer, L. Bellis, R. Yates, and M. Barr, Raytheon long life cryocoolers for future space missions, Cryogenics **88**, 44 (2017).